



Trans. Nonferrous Met. Soc. China 24(2014) 3492-3499

Transactions of Nonferrous Metals Society of China

www.tnmsc.cn

Processing map and hot deformation mechanism of novel nickel-free white copper alloy

Na LIU ^{1,2}, Zhou LI ^{1,3}, Ling LI ¹, Bin LIU ¹, Gen-ying XU ¹

- 1. School of Materials Science and Engineering, Central South University, Changsha 410083, China;
- 2. Key Laboratory of Nonferrous Metal Materials Science and Engineering, Ministry of Education, Central South University, Changsha 410083, China;
- 3. State Key Laboratory of Powder Metallurgy, Central South University, Changsha 410083, China

Received 6 November 2013; accepted 24 March 2014

Abstract: Hot compression test of a novel nickel-free white alloy Cu-12Mn-15Zn-1.5Al-0.3Ti-0.14B-0.1Ce (mass fraction, %) was conducted on a Gleeble-1500 machine in the temperature range of 600-800 °C and the strain rate range of 0.01-10 s⁻¹. The constitutive equation and hot processing map of the alloy were built up according to its hot deformation behavior and hot working characteristics. The deformation activation energy of the alloy is 203.005 kJ/mol. An instability region appears in the hot deformation temperature of 600-700 °C and the strain rate range of 0.32-10 s⁻¹ when the true strain of the alloy is up to 0.7. Under the optimal hot deformation condition of 800 °C and 10 s⁻¹ the prepared specimen has good surface quality and interior structure. The designed nickel-free alloy has very similar white chromaticity with the traditional white copper alloy (Cu-15Ni-24Zn-1.5Pb), and the color difference between them is less than 1.5, which can hardly be distinguished by human eyes.

Key words: Ni-free white copper alloy; hot compression deformation; constitutive equation; processing map

1 Introduction

Nickel is often used as a key element to produce white copper alloys as it can change the color of copper alloys from red to white [1]. Nickel-containing white copper alloy has been widely used to produce coin, button, zipper, spectacles frame, watchcase, necklace and artwork, due to their silver color, good process ability, favorable cutting performance, fine anti-tarnish property and excellent corrosion resistance [2,3]. However, nickel is harmful to human health, and it may cause allergic by contacting with skin [4-7]. European and American countries have recently forbidden the application of nickel-containing products, and the rule about the content and release amount of nickel in products is getting stricter [8-10]. In order to replace the element nickel, the Japanese YKK Corporation has developed two nickel-free copper alloys, Cu-Zn-Mn and Cu-Zn-Ti [11-13]. They also made analysis on the heat

mechanical treatment, property cracking susceptibility. Only the values of a^* and b^* that present the color degree were used to describe the alloy chromaticity. The third value L^* that denotes the quality of lighting was ignored. In fact, L^* is the key parameter that determines alloy grey scale. Copper alloy has no white in its appearance as L^* drops under 70, no matter how closely a^* and b^* approach zero [14]. Meanwhile, there is no report from YKK about the research on their deformability and process technology. Hot deformation is such an important process that completely eliminates the dendrite structure in cast alloy, generates fine and uniform recrystallized grains, and greatly improves the mechanical properties and corrosion resistance of the alloy [15,16].

In this work, the hot deformation process of the designed Cu-12Mn-15Zn-1.5Al-0.3Ti-0.14B-0.1Ce (mass fraction, %) alloy with fine white chromaticity was investigated at different temperatures and strain rates using hot compression simulation. The constitutive

Foundation item: Project (51271203) supported by the National Natural Science Foundation of China; Project (CX2012B037) supported by the Hunan Provincial Innovation Foundation for Postgraduate, China; Project (2013zzts017) supported by the Graduate Degree Thesis Innovation Foundation of Central South University, China; Project (2012bjjxj015) supported by the Excellent Doctor Degree Thesis Support Foundation of Central South University, China

Corresponding author: Zhou LI; Tel: +86-731-88830264; Fax: +86-731-88876692; E-mail: lizhou6931@csu.edu.cn DOI: 10.1016/S1003-6326(14)63493-2

equation and processing map of the alloy were established and the microstructure evolution during the hot-compression process was characterized.

2 Experimental

The designed Cu-12Mn-15Zn-1.5Al-0.3Ti-0.14B-0.1Ce alloy was prepared by traditional casting method and the traditional nickel white copper alloy (Cu-15Ni-24Zn-1.5Pb) was selected as a reference. The compositions of two alloys are listed in Table 1. The samples were cut into $d10 \text{ mm} \times 15 \text{ mm}$ specimens for hot simulation test, which was conducted on a Gleeble-1500 machine at temperatures of 600, 650, 700, 750 and 800 °C and strain rates of 0.01, 0.1, 1 and 10 s⁻¹, respectively. The total hot deformation was 70%. After hot deformation the specimen was quenched by cold water immediately so that the hot deformed structure could be preserved. HP 200 precision color difference instrument was used to test the burnished alloy surface, and CIE1976LAB standard was applied to testing and calculating. Color difference was calculated based on the chromaticity of Cu-15Ni-24Zn-1.5Pb alloy surface, expressed as $\Delta E^* = [(L_d^* - L_w^*)^2 + (a_d^* - a_w^*)^2 + (b_d^* - b_w^*)^2]^{1/2}$ where L^* is the lightness, a^* is the red-green opponent, b^* is the yellow-blue opponent, subscripts d and w designate the designed sample and the traditional white copper, respectively. The microstructure was observed by a Leica EC3 metallurgical microscope.

Table 1 Compositions of designed alloy and referred alloy

Alloy	Mass fraction/%									
	Mn	Zn	Al	Ti	В	Ce	Ni	Pb	Cu	
Cu-12Mn-15Zn-										
1.5Al-0.3Ti-	12	15	1.5	0.3	0.14	0.1	_	_	Bal.	
0.14B-0.1Ce										
Cu-15Ni-	Cu-15Ni- 24Zn-1.5Pb - 2	24	_	_	-	-	15	1.5	Bal.	
24Zn-1.5Pb		∠4								

3 Results and discussion

3.1 Chromaticity and color difference

Table 2 shows the white chromaticity and color difference results of the designed and referred alloys. It

 Table 2 Chromaticity parameters and color differences of designed alloy and referred alloy

		-	Color difference		
L^*	a*	b^*	ΔE^*		
86.45	-0.05	7 14	1.28		
80.43	0.03	7.14	1.20		
87.50	0.26	6.48	_		
	L* 86.45	$ \begin{array}{ccc} paramete \\ L^* & a^* \\ 86.45 & -0.05 \end{array} $	Chromaticity parameter $L^* = a^* = b^*$ 86.45 -0.05 7.14 87.50 0.26 6.48		

can be seen that the two alloys have very similar white chromaticity. The color difference between them is less than 1.5, which can hardly be distinguished by human eyes.

3.2 Microstructure of as-cast alloy

The typical microstructure of the as-cast Cu-12Mn-15Zn-1.5Al-0.3Ti-0.14B-0.1Ce alloy before hot deformation is shown in Fig. 1, indicating that well-developed dendritic structure can be observed in grains.

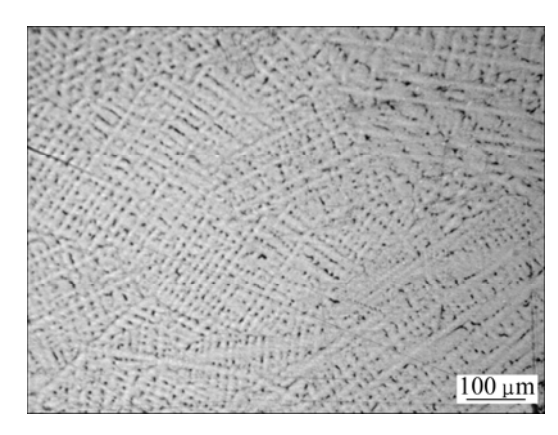


Fig. 1 Initial microstructure of as-cast Cu-12Mn-15Zn-1.5Al-0.3Ti-0.14B-0.1Ce alloy before hot deformation

3.3 Stress-strain behavior

Figure 2 shows the true stress-true strain curves of the designed alloy during hot deformation at different temperatures and strain rates. It can be seen that both deformation temperature and strain rate have great influence on alloy rheological behavior. At the same strain rate, the true stress decreases with increasing deformation temperature; while at the same deformation temperature, the true stress increases with increasing strain rate. Besides, the maximum true stress and the steady true stress both increase with the increase of strain rate and the decrease of deformation temperature, which can be attributed to a process balanced by work-hardening and dynamic recrystallization softening during hot compression. At high deformation temperatures (750-800 °C) and low strain rates (0.01-0.1 s⁻¹), the alloy can obtain enough heat energy or deformation energy. As the work-hardening made the true strain approach its top value, dynamic recrystallization occurred and soon got balanced with work-hardening, keeping the true stress stable [17,18]. Under other conditions, the dynamic recrystallization will not happen or could not happen completely because of insufficient energy, or energy releasing by dynamic recovery. The curves of true stress-strain demonstrated the difficulty to approach a dynamic balance.

3.4 Constitutive relation model

Constitutive relation is often used to describe the plastic deformation of metallic material [19,20]:

$$\dot{\varepsilon} = A[\sinh(\alpha\sigma)]^n \exp[-Q/(RT)] \tag{1}$$

where A, α and n are constants unrelated to temperature; $\dot{\varepsilon}$ is the strain rate; σ is the flow stress; Q is the activation energy for deformation; R is the gas and constant; T is the Kelvin temperature. At different flow stresses, Eq. (1) can be expressed in different forms [21,22]:

$$\dot{\varepsilon} = B\sigma^{n_1} \exp[-Q/(RT)], \ \alpha\sigma < 0.8 \tag{2}$$

$$\dot{\varepsilon} = C \exp(\beta \sigma) \exp[-Q/(RT)], \alpha \sigma > 1.2 \tag{3}$$

where B, C, n_1 and β are constants and $\alpha = \beta/n_1$. Taking natural logarithm on Eqs. (2) and (3), we obtain

$$\ln \dot{\varepsilon} = \ln B + n_1 \ln \sigma - Q/(RT) \tag{4}$$

$$\ln \dot{\varepsilon} = \ln C + \beta \sigma - Q/(RT) \tag{5}$$

Equations (4) and (5) indicate that the slopes of $\ln \dot{\varepsilon} - \ln \sigma$ and $\ln \dot{\varepsilon} - \sigma$ are n_1 and β , respectively, which can be obtained from Figs. 3(a) and (b) by linear regression, 6.444 and 0.0417. Then, α =0.00647.

Taking natural logarithm on Eq. (1), we get

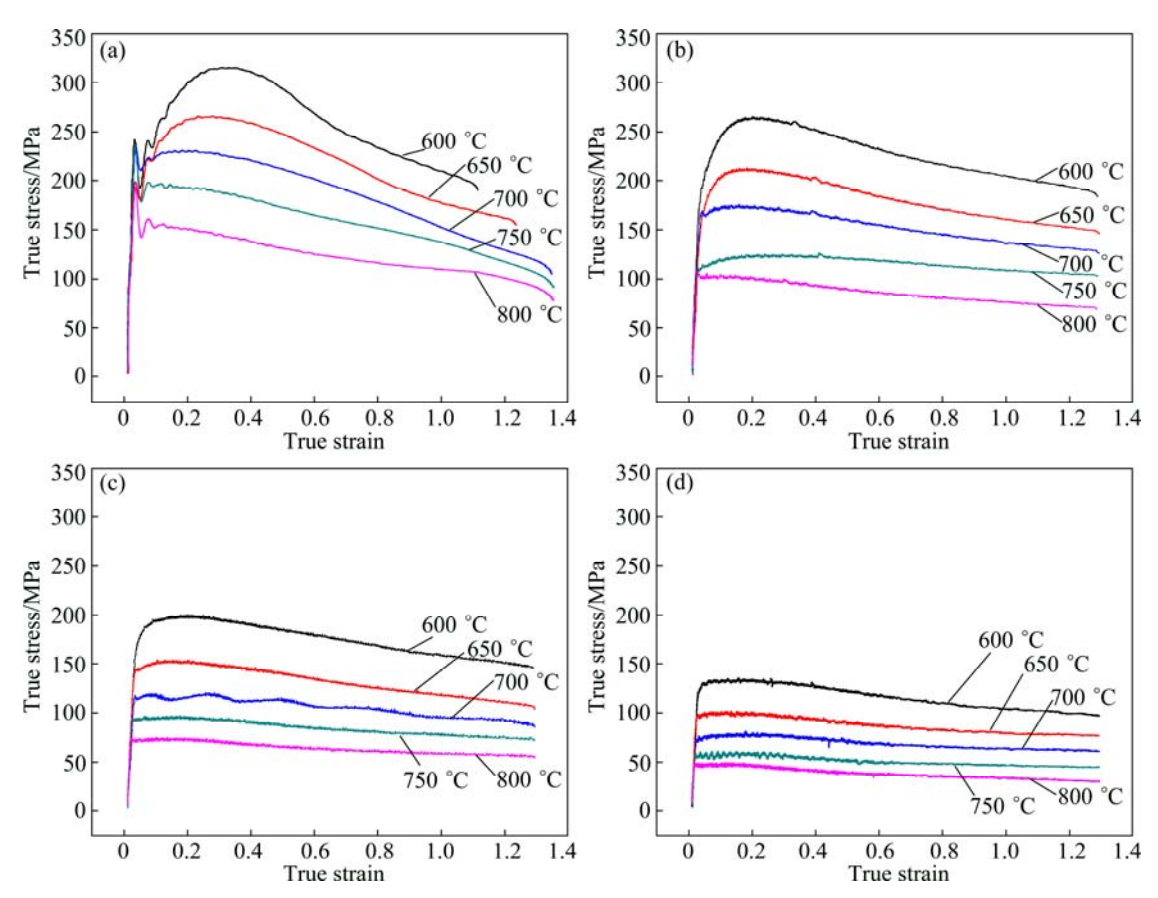


Fig. 2 True stress-strain curves of Cu-12Mn-15Zn-1.5Al-0.3Ti-0.14B-0.1Ce alloy deformed at different strain rates: (a) 10 s^{-1} ; (b) 1 s^{-1} ; (c) 0.1 s^{-1} ; (d) 0.01 s^{-1}

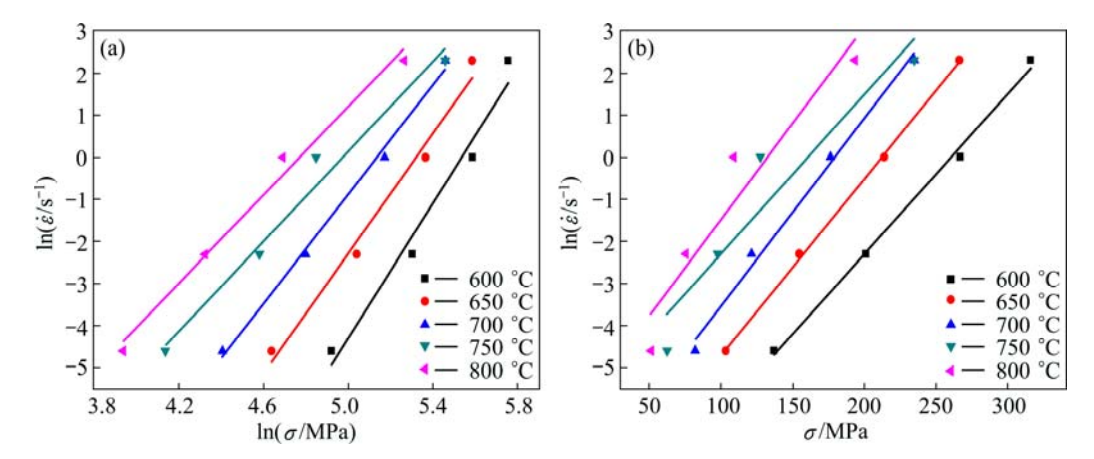


Fig. 3 Relationship between strain rate and flow stress: (a) $\ln \dot{\varepsilon} - \ln \sigma$; (b) $\ln \dot{\varepsilon} - \sigma$

$$\ln \dot{\varepsilon} = \ln A + n \ln[\sinh(\alpha\sigma)] + [-Q/(RT)] \tag{6}$$

Derivation of Eq. (6) is shown as follows:

$$Q = 1000R \left\{ \frac{\partial \ln \dot{\varepsilon}}{\partial \ln \left[\sinh \left(\alpha \sigma \right) \right]} \right\}_{T}.$$

$$\left\{ \frac{\partial \ln \left[\sinh \left(\alpha \sigma \right) \right]}{\partial \left(1000/T \right)} \right\}_{\dot{\varepsilon}} = 1000RnS \tag{7}$$

Figure 4 shows the results of $\ln \dot{\varepsilon}$ vs $\ln[\sinh(\alpha\sigma)]$ and $\ln[\sinh(\alpha\sigma)]$ vs T^{-1} . Substituting the slope coefficient of curves shown in Fig. 4 into Eq. (7), we get the activation energy Q=203.005 kJ/mol and n=4.786.

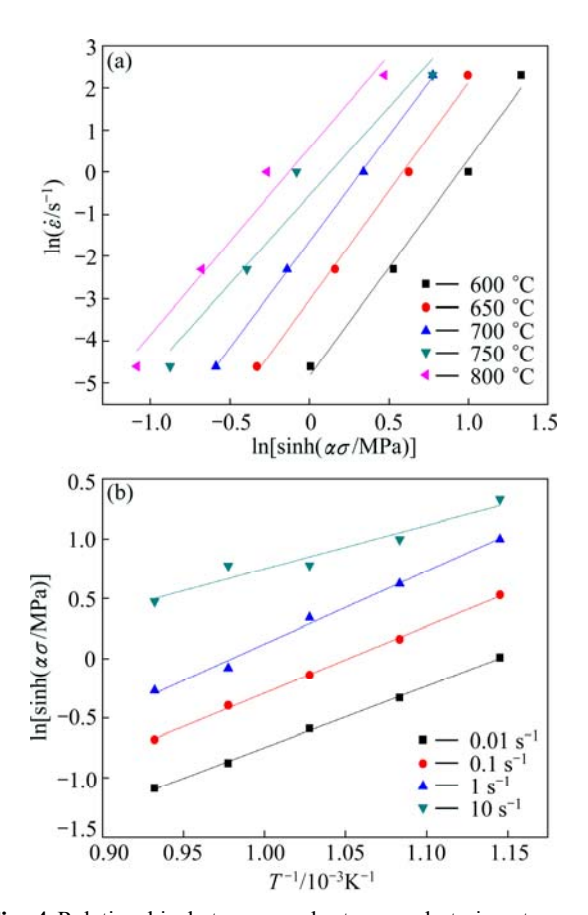


Fig. 4 Relationship between peak stress and strain rate, peak stress and deformation temperature: (a) $\ln \dot{\varepsilon} - \ln[\sinh(\alpha\sigma)]$; (b) $\ln[\sinh(\alpha\sigma)] - T^{-1}$

In order to resolve Eq. (1) at hot processing more efficiently, the Zener-Hollomon coefficient was introduced to transform Eq. (1) to Eqs. (8) and (9) [23]:

$$Z = \dot{\varepsilon} \exp[Q/(RT)] = A[\sinh(\alpha\sigma)]^n$$
 (8)

$$ln Z = ln A + n ln[sinh(\alpha\sigma)]$$
 (9)

Figure 5 shows the relationship between $\ln Z$ and $\ln[\sinh(\alpha\sigma)]$, with slope coefficient n of 4.739 and intercept $\ln A$ of 23.481. This shows that the values of n calculated by Eqs. (7) and (9) are close to each other.

Taking their average value of 4.763 back into Eq. (1), the constitutive equation of the designed alloy can be expressed as

$$\dot{\varepsilon} = e^{23.481} \left[\sinh(0.00647\sigma) \right]^{4.763} \exp[-203.005/(RT)]$$
(10)

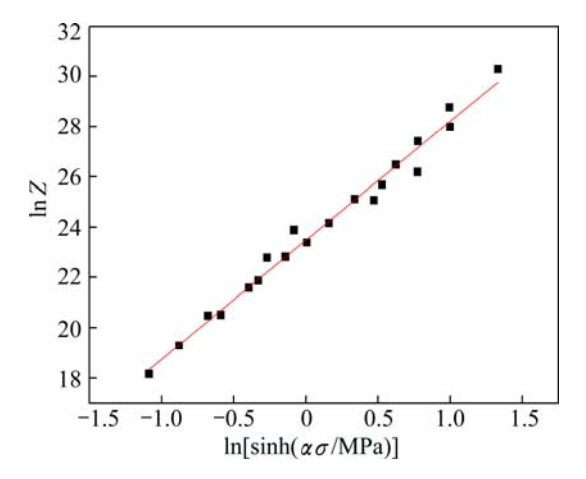


Fig. 5 Relationship between parameter Z and peak stress

3.5 Processing map

During the hot processing, power P consists of two parts, G and J, the former consumed by plastic deformation and the latter consumed by structure change. Their relationship can be described as [24,25]

$$P = \sigma \dot{\varepsilon} = G + J = \int_{0}^{\dot{\varepsilon}} \sigma d\dot{\varepsilon} + \int_{0}^{\sigma} \dot{\varepsilon} d\sigma$$
 (11)

$$\left(\frac{\partial J}{\partial G}\right)_{\varepsilon,T} = \frac{\partial P}{\partial G}\frac{\partial J}{\partial P} = \frac{\sigma d\dot{\varepsilon}}{\dot{\varepsilon} d\sigma} = \left[\frac{\partial (\ln \sigma)}{\partial (\ln \dot{\varepsilon})}\right]_{\varepsilon,T} = m \tag{12}$$

where m is the sensitive factor of strain rate.

KLEEMOLA and NIEMINEN [26], and PRASAD [27,28] reported that there was a relationship between stress σ and strain rate $\dot{\varepsilon}$ in hot deforming part at given temperature and strain:

$$\sigma = K \dot{\varepsilon}^m \tag{13}$$

Combining Eqs. (11), (12) and (13), the following equation can be gained:

$$J = \sigma \dot{\varepsilon} - \int_0^{\dot{\varepsilon}} K \dot{\varepsilon}^m d\dot{\varepsilon} = \frac{m}{m+1} \sigma \dot{\varepsilon}$$
 (14)

For material in an ideal linear dissipative state, m=1 and $J_{\text{max}}=J_{(m=1)}=\sigma \dot{\varepsilon}/2=P/2$. Power dissipation factor η is defined as [29]

$$\eta = \frac{J}{J_{\text{max}}} = \frac{2m}{m+1} \times 100\% \tag{15}$$

 η can effectively reflect the deformation mechanism of material microstructure at given temperature and strain rate [25]. The relationship among η , deformation temperature and strain rate can be illustrated in the power dissipation map.

Based on irreversible thermodynamics extremum

principle, the instability map can be applied as a continuous instability criterion by using dimensionless factor $\xi(\dot{\varepsilon})$ to describe large plastic deformation. PRASAD and SESHACHARYULU [30], and ZHANG et al [31] deduced the instability criterion expression of materials by the following the maximum entropy principle:

$$\xi(\dot{\varepsilon}) = \frac{\partial \ln[m/(m+1)]}{\partial \ln \dot{\varepsilon}} + m < 0 \tag{16}$$

Figure 6 shows the processing maps of the designed alloy at true strains of 0.5 and 0.7, in which the dashed area is the instability region. Two dissipation maps at true strains of 0.5 and 0.7 are similar. The maximum dissipation factor at true strain of 0.7 is slightly smaller than that at true strain of 0.5. At true strain of 0.5, there is no instability region. As the true strain rises up to 0.7, the value of $\xi(\dot{\varepsilon})$ falls below zero in the regions of low temperature and high strain rate. The instability region is defined in the deformation temperature range of 600-700 °C and the strain rate range of 0.32-10 s⁻¹. The microstructure of the instability region is shown in Fig. 7. It can be seen from Fig. 7 that the deformation at this moment is not uniform. The as-cast dendrite (shown in Fig. 1) is not eliminated completely, adiabatic shear bands generate under both deformation conditions, and cracks appear in the alloy at a low deformation temperature of 600 °C, as shown in Fig. 7(a).

At true strain of 0.7, the dissipation factor η outside the instability region is all larger than 0.35, which illustrates that the dynamic recrystallization occurs in this region [30]. Figure 8 shows the microstructures of this region under two deformation conditions. It can be seen that the as-cast structure is wholly eliminated, and some tiny recrystallized grains are generated between shear zones during the deformation process. On the hot processing map shown in Fig. 6(b), the dissipation factor η increases up to 0.65 in the deformation temperature range of 700-800 °C and the strain rate range of 0.01-0.032 s⁻¹, probably initiating the superplastic deformation [30]. Recrystallization takes place at the beginning stage of hot deformation. The as-cast structure transfers into tiny recrystallization grains, and finally becomes superplastic in the later deformation process. The microstructure of the alloy is shown in Fig. 9(a) after hot compression under deformation conditions of 800 °C and 0.01 s^{-1} . No dendrite is observed, and the microstructure of the deformed alloy transfers into tiny and even recrystallized grain. In order to improve the product efficiency, high deformation rate is always used in industry production. High dissipation factor η can be found in Fig. 6(b) at the strain rate of 10 s⁻¹ and the

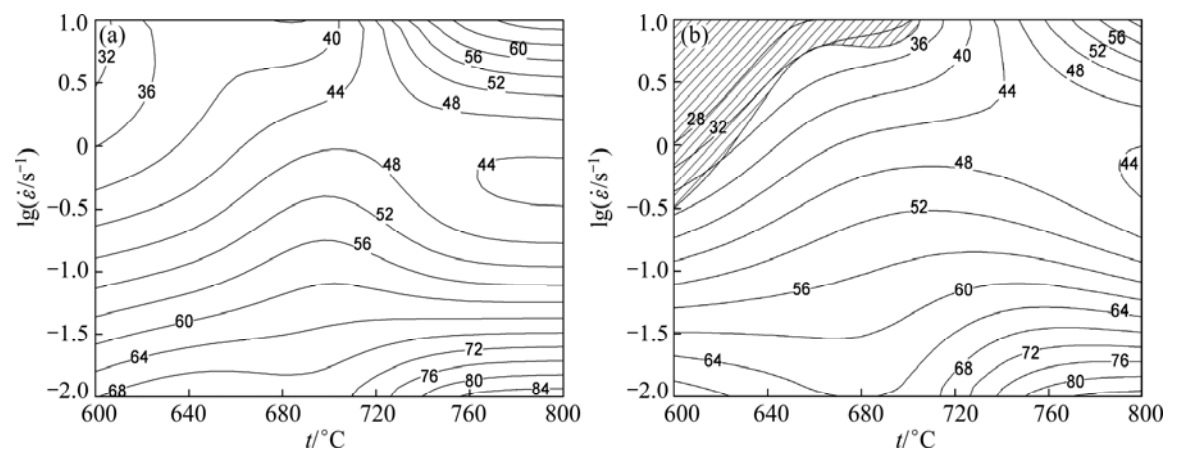


Fig. 6 Processing maps of Cu-12Mn-15Zn-1.5Al-0.3Ti-0.14B-0.1Ce alloy at different strains: (a) ε =0.5; (b) ε =0.7

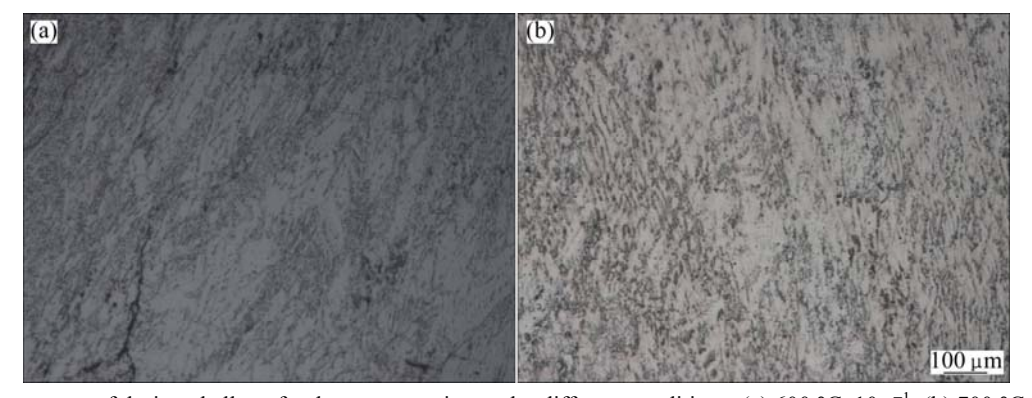


Fig. 7 Microstructures of designed alloy after hot compression under different conditions: (a) 600 °C, 10 s⁻¹; (b) 700 °C, 10 s⁻¹

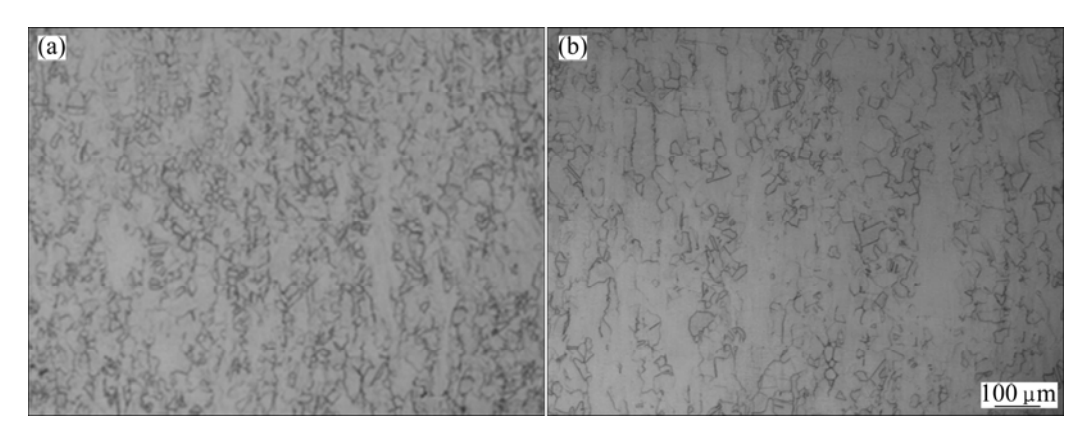


Fig. 8 Microstructures of designed alloy after hot compression under different conditions: (a) 700 °C, 0.1 s⁻¹; (b) 750 °C, 0.1 s⁻¹

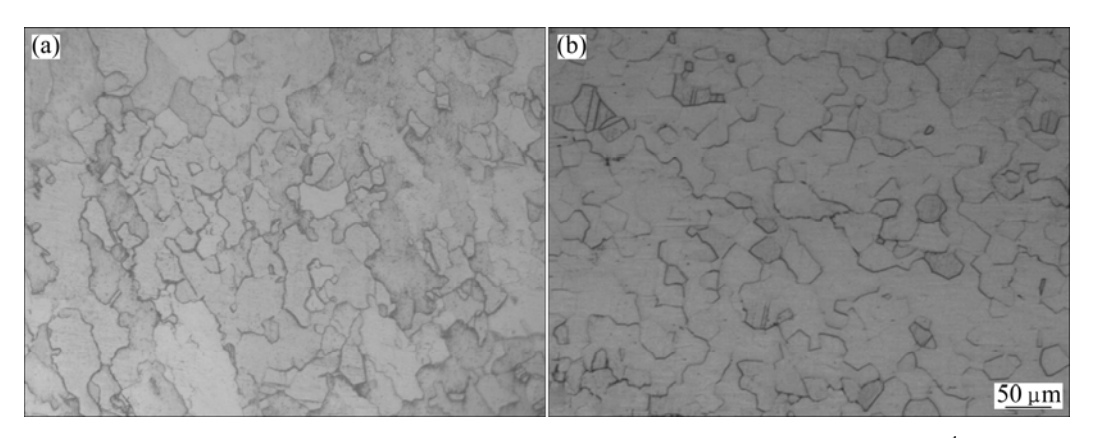


Fig. 9 Microstructures of designed alloy after hot compression under different conditions: (a) 800 °C, 0.01 s⁻¹; (b) 800 °C, 10 s⁻¹

deformation temperature of 750-800 °C. The microstructure of the alloy under the deformation condition of 800 °C and 10 s^{-1} is shown in Fig. 9(b), illustrating that fine dynamic recrystallization structure can be obtained in the alloy deformed under this condition.

3.6 Hot rolling test

The designed alloy specimens were kept at 800 °C for 2 h, and then hot rolled on double rolling mill. Figure 10 shows the macrophotograph of the hot-rolled sheet, revealing that no crack can be seen on the surface. The typical longitudinal section micrograph of the hot-rolled sheet is shown in Fig. 11, indicating that the dynamic recrystallization occurs, and no crack is observed after hot rolling.



Fig. 10 Macrophotograph of designed alloy after hot rolling at $800~^{\circ}\text{C}$ and $10~\text{s}^{-1}$

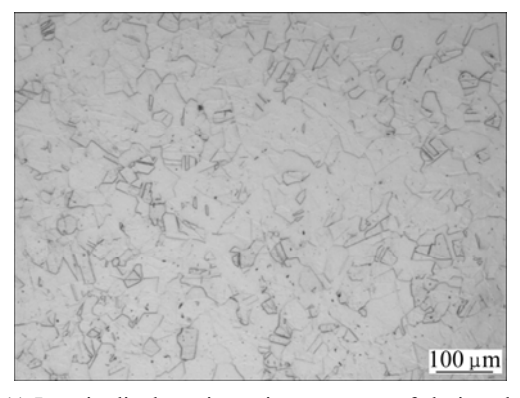


Fig. 11 Longitudinal section microstructure of designed alloy after hot rolling at 800 $^{\circ}\text{C}$ and 10 s^{-1}

4 Conclusions

- 1) Cu-12Mn-15Zn-1.5Al-0.3Ti-0.14B-0.1Ce alloy has a fine white chromaticity (a^* =-0.05, b^* =7.14, L^* =86.45), with color difference smaller than 1.5 compared with traditional white Cu-15Ni-24Zn-1.5Pb alloy.
- 2) Detailed values of parameter in constitutive relation model are computed. The activity energy Q is 203.005 kJ/mol, and the constitutive relation is expressed as

- $\dot{\varepsilon} = e^{23.481} \left[\sinh(0.00647\sigma) \right]^{4.763} \exp[-203.005/(RT)].$
- 3) The processing map of Cu-12Mn-15Zn-1.5Al-0.3Ti-0.14B-0.1Ce alloy is established. At true strain of 0.7, an instability zone is found. The deformation temperature range is from 600 to 700 °C and the strain rate range is from 0.32 to $10~\rm s^{-1}$.

References

- [1] ANSUINI F J, BADIA F A. High strength microduplex Cu-Ni-Zn alloys [J]. Metallurgical Transactions, 1973, 4: 15–20.
- [2] SUBRAMANIAN V, CHANDRAMOHAN P, SRINIVASAN M P, VELMURUGAN S, NARASIMHAN S V. Corrosion of cupronickel alloy in permanganate under acidic condition [J]. Corrosion Science, 2007, 49: 620–636.
- [3] ALLAM N K, HEGAZY H S, ASHOUR E A. Inhibition of the sulfide induced pitting of copper nickel alloy using benzotriazole [J]. Internation! Journal of Electrochemical Science, 2007, 2: 549–562.
- [4] LIDEN C, SKARE L, VAHTER M. Release of nickel from coins and deposition onto skin from coin handling-comparing euro coins and SEK [J]. Contact Dermatitis, 2008, 59: 31–37.
- [5] NESTLE F O, SPEIDEL H, SPEIDEL M O. High nickel release from 1- and 2-Euro coins [J]. Nature, 2002, 419(6903): 132.
- [6] DAS K K, DAS N, DHUNDASI S A. Nickel, its adverse health effects & oxidative stress [J]. Indian J Med Res, 2008, 128: 412–425.
- [7] LIDÉN C, MENNÉ T, BURROWS D. Nickel-containing alloys and platings and their ability to cause dermatitis [J]. British Journal of Dermatology, 1996, 134: 193–198.
- [8] CEMPEL M, NIKEL G. Nickel: A review of its sources and environmental toxicology [J]. Polish Journal of Environmental Studies, 2006, 15(3): 375–382.
- [9] SCOOTT-FORDSMAND J J. Toxicity of nickel to soil organisms in Denmark [J]. Reviews of Environmental Contamination and Toxicology, 1997, 148: 1–34.
- [10] COOGAN T T, LATTA D M, SNOW E T, COSTA M. Toxicity and carcinogenicity of nickel compounds [J]. Crit Rev Toxicol, 1989, 19(4): 341–384.
- [11] YOSHIMURA Y, KITA K, INOUE A. Development of novel nickel free white Cu alloys [J]. Journal of Japan Research Institute for Advanced Copper, 2004, 43: 291–295.
- [12] YOSHIMURA Y, KITA K, INOUE A. White-color Cu–Zn–Mn alloys with low season cracking susceptibility [J]. Journal of the Society of Materials Science, 2004, 53(2): 188–192.
- [13] YOSHIMMURA Y, KITA K, INOUE A. Mechanical properties and microstructure of new Ni free white Cu alloy [J]. Materials Science Forum, 2003, 426–432: 3359–3364.
- [14] GB/T 7921–2008. Uniform color space and color difference formula [S]. 2008. (in Chinese)
- [15] LU Yan-ling, LIU Jin-xi, LI Xiao-ke, LIANG Jian-ping, LI Zhi-jun, WU Guan-yuan, ZHOU Xing-tai. Hot deformation behavior of Hastelly C276 superalloy [J]. Transactions of Nonferrous Metals Society of China, 2012, 22(S1): s84–s88.

- [16] ZHU Aa-yin, CHEN Jing-lin, LI Zhou, LUO Li-yang, LEI Qian, ZHANG Liang, ZHANG Wan. Hot deformation behavior of novel imitation-gold copper alloy [J]. Transactions of Nonferrous Metals Society of China, 2013, 23: 1349–1355.
- [17] CAI Da-yong, XIONG Liang-yin, LIU Wen-chang, SUN Gui-dong, YAO Mei. Characterization of hot deformation behavior of a Ni-base superalloy using processing map [J]. Materials and Design, 2009, 30: 921–925.
- [18] CHEN Hui-qin, CAO Chun-xiao. Characterization of hot deformation microstructures of alpha-beta titanium alloy with equiaxed structure [J]. Transactions of Nonferrous Metals Society of China, 2012, 22: 503-509.
- [19] SELLARS C M, TEGART W J M. Hot workability [J]. International Metallurgical Reviews, 1972, 17(1): 1–24.
- [20] SELLARS C M, MCTEGART W J. On the mechanism of hot deformation [J]. Acta Metallurgica, 1966, 14: 1136–1138.
- [21] ZHANG L, LI Z, LEI Q, QIU W T, LUO H T. Hot deformation behavior of Cu-8.0Ni-1.8Si-0.15Mg alloy [J]. Materials Science & Engineering A, 2011, 528: 1641-1647.
- [22] LU Shi-qiang, LI Xin, WANG Ke-lu, DONG Xian-juan, FU M W. High temperature deformation behavior and optimization of hot compression process parameters in TC11 titanium alloy with coarse lamellar original microstructure [J]. Transactions of Nonferrous Metals Society of China, 2013, 23: 353–360.
- [23] LI H Z, WANG H J, LIANG X P, LIU H T, LIU Y, ZHANG X M. Hot deformation and processing map of 2519A aluminum alloy [J]. Materials Science and Engineering A, 2011, 528: 1548–1552.
- [24] PRASAD Y V R K, SASIDHARA S. Hot working guide: A compendium of processing maps [M]. OH: ASM International, 1997.
- [25] PRASAD Y V R K, GEGEL H L, DORAIVELU S M, MALAS J C, MORGAN J T, LARK K A, BARKER D R. Modeling of dynamic material behavior in hot deformation: Forging of Ti-6242 [J]. Metallurgical Transactions, 1984, 15: 1883–1892.
- [26] KLEEMOLA H J, NIEMINEN M A. On the strain-hardening parameters of metals [J]. Metallurgical Transactions, 1974, 5: 1863–1866.
- [27] PRASAD Y V R K, SESHACHARYULU T. Processing maps for hot working of titanium alloys [J]. Materials Science and Engineering A, 1998, 243: 82–88.
- [28] SIVAKESAVAM O, PRASAD Y V R K. Hot deformation behaviour of as-cast Mg-2Zn-1Mn alloy in compression: A study with processing map [J]. Materials Science and Engineering A, 2003, 362: 118-124.
- [29] RAVICHANDRAN N, PRASAD Y V R K. Dynamic recrystallization during hot deformation of aluminum: A study using processing maps [J]. Metallurgical Transactions A, 1991, 22: 2339–2348.
- [30] PRASAD Y V R K, SESHACHARYULU T. Modellong of hot deformation for microstructure control [J]. International Materials Reviews, 1998, 43(6): 243–258.
- [31] ZHANG Yi, LIU Ping, TIAN Bao-hong, LIU Yong, LI Rui-qin, XU Qian-qian. Hot deformation behavior and processing map of Cu–Ni–Si–P alloy [J]. Transactions of Nonferrous Metals Society of China, 2013, 23: 2341–2347.

新型无镍白色铜合金的 热加工图及其热变形机制

刘娜1,2,李周1,3,李灵1,刘斌1,徐根应1

- 1. 中南大学 材料科学与工程学院,长沙 410083;
- 2. 中南大学 有色金属材料科学与工程教育部重点实验室,长沙 410083;
 - 3. 中南大学 粉末冶金国家重点实验室,长沙 410083;

摘 要: 采用 Gleeble-1500 热模拟实验机在温度为 600~800 °C、应变速率为 0.01~10 s⁻¹ 的热变形条件下对新型无镍白色 Cu-12Mn-15Zn-1.5Al-0.3Ti-0.14B-0.1Ce(质量分数,%)合金进行热压缩模拟实验;根据该合金热变形行为及热加工特征,建立该合金热变形的本构方程和热加工图。该合金热变形过程中变形激活能为 203.005 kJ/mol。当真应变为 0.7 时,合金热加工图中存在一个失稳区,此区域的变形温度为 600~700 °C,应变速率为 0.32~10 s⁻¹。在较适宜的热变形条件(800 °C、10 s⁻¹)下获得的合金具有良好的表面质量和内部组织。同时,该无镍合金具有与传统镍白铜 Cu-15Ni-24Zn-1.5Pb 合金相近似的白色色度和肉眼不易察觉的色差(小于 1.5)。

关键词: 无镍白色铜合金; 热压缩变形; 本构方程; 加工图

(Edited by Wei-ping CHEN)